RESEARCH ARTICLE | JUNE 02 2025

## Dynamic fluctuations in a highly cross-linked polybutadiene rubber

Benedetta P. Rosi ( ); Margarita Kruteva ( ); Michael Monkenbusch ( ); Jürgen Allgaier ( ); Peter Falus ( ); Jacques Ollivier ( ); Nicolas R. de Souza ( ); Dieter Richter ( )



J. Chem. Phys. 162, 214902 (2025) https://doi.org/10.1063/5.0265589





#### Articles You May Be Interested In

Effect of binding to carbon black on the dynamics of 1,4-polybutadiene

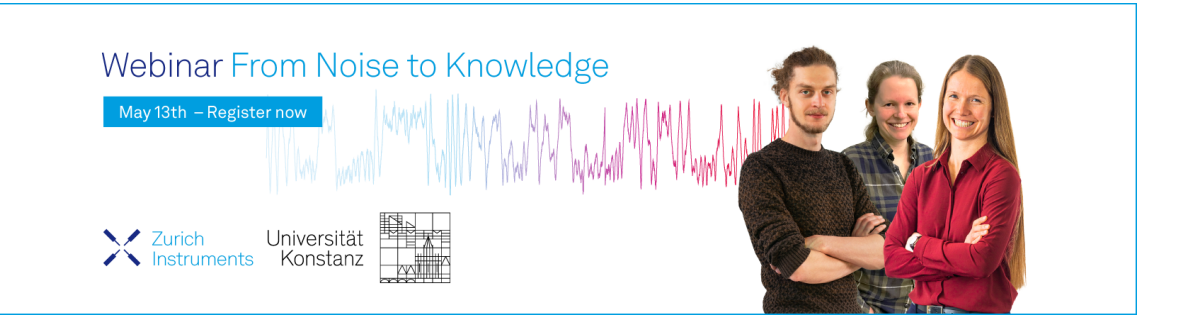
J. Chem. Phys. (October 2013)

Influence of the microstructure on the incoherent neutron scattering of glass-forming polybutadienes

J. Chem. Phys. (July 1996)

Coarse-grained simulations of cis- and trans-polybutadiene: A bottom-up approach

J. Chem. Phys. (February 2017)





# Dynamic fluctuations in a highly cross-linked polybutadiene rubber

Cite as: J. Chem. Phys. 162, 214902 (2025); doi: 10.1063/5.0265589

Submitted: 14 February 2025 • Accepted: 6 May 2025 •

**Published Online: 2 June 2025** 







#### **AFFILIATIONS**

- <sup>1</sup> Jülich Centre for Neutron Science, Forschungszentrum Julich GmbH, 52428 Julich, Germany
- <sup>2</sup>Institut Laue-Langevin (ILL), 38000 Grenoble, France
- <sup>3</sup>Australian Nuclear Science and Technology Organisation, Lucas Heights, Sydney, New South Wales 2234, Australia
- a) Present address: European Spallation Source ERIC, 224 84 Lund, Skåne County, Sweden.

  Author to whom correspondence should be addressed: benedetta.rosi@ess.eu

#### **ABSTRACT**

Using a combined approach of different neutron scattering techniques that allows experimental separation of the self and collective dynamics, we investigated the various types of motion in a highly cross-linked 1,2-polybutadiene rubber. As a reference, the neat, fully deuterated melt was also studied. In the latter, the collective segmental relaxation around the structure factor peak  $S(Q_{max})$  exhibits pronounced de Gennes narrowing, with a collective relaxation time  $\tau_c(Q)$  that increases without plateauing toward lower momentum transfers Q. Apparently, due to the very bulky monomer structure, the correlation length  $\xi_c$  for the crossover to viscoelastic homogeneity is unusually large. In the highly cross-linked d1,2-PB rubber, the original structure factor peak of the pure d1,2-PB is significantly reduced. Instead, a strong low-Q peak emerges, which we attribute to correlations between the hydrogen-containing cross-linkers. Both the collective d1,2-PB relaxation rates around the former  $S(Q_{max})$  and the relaxation around the new crosslink correlation peak are significantly slowed down compared to the neat melt. Finally, the cross-linking strands exhibit their own fast dynamics, which is well described by diffusion within a spherical Gaussian well, with a corresponding radius  $R \cong 4$  Å.

© 2025 Author(s). All article content, except where otherwise noted, is licensed under a Creative Commons Attribution (CC BY) license (https://creativecommons.org/licenses/by/4.0/). https://doi.org/10.1063/5.0265589

#### I. INTRODUCTION

Cross-linked polymers represent a broad class of materials with enormous societal impact. They are broadly used in the tire industry, as coating, adhesives, seals, and membranes. <sup>1-3</sup> For instance, when the stress on the rubber product is released, the cross-links are responsible for instantaneous recovery to the shape of tires. The unusual elasticity of rubber-like materials originates from their cross-linked polymeric structure. The structure of cross-linked polymers has been extensively studied because they exhibit strong reinforcement properties even without added fillers like carbon black, silica, or clay.

In general, cross-linkers of different origin represent a means to tune the cross-linked rubber-like materials. In this context, metallic moieties forming tens of nanometres scale aggregates play an important role in manufacturing lightweight and mechanically robust materials with excellent reinforcement properties.<sup>4</sup>

The relationship between the structure and density of cross-linking junctions and mechanical properties of rubbers has been studied extensively.<sup>5</sup> It has been concluded that network junctions reduce the motional freedom and mobility of the polymer chains and cause an increase of the glass transition temperature  $(T_g)$ .<sup>6</sup> In addition, strong connectivity between all chains leads to collective behavior. In cross-linked poly(vinyl ethylene) (PVE), slower relaxation times and inhomogeneous broadening of the associated relaxation functions on increasing cross-linking density are observed by broadband dielectric spectroscopy.<sup>6</sup> Similarly, cross-linked PMMA demonstrates broadened mechanical spectra and increased fragility.<sup>7</sup>

Various simulations on mechanical network properties are described in the literature. One of the earliest simulations examined the dynamic modulus and dynamic structure factor for different components. A plateau-like behavior was observed for both functions already at very short observation times.<sup>8</sup> Network

formation kinetics and stress-strain behavior in end-linked poly(dimethylsiloxane) (PDMS) studied by molecular dynamics simulations demonstrate that networks are deformed much more affinely than what appears to be seen experimentally. In addition, the effect of entanglements was investigated. In the results indicate that the entanglements affect the network elastic response at both small and large extensions. Study of temperature effects in cross-linked polymers showed that the time-temperature superposition (TTSP) works on segmental level. 12

Results by Liu et al. consider the dependence of structure and dynamics of elastomer networks as a function of cross-link density.<sup>13</sup> They found that introducing 6% cross-links does not show any effect on the static structure factor of the cross-linked systems. However, at this concentration, the glass transition temperature  $T_g$  of the cross-linked network increases by about 20% compared to the neat polymer. This phenomenon is related to the restricted segmental mobility in the vicinity of the cross-links. At short times, retarded segmental diffusivity at higher cross-link density was observed. The segmental mean squared displacement (MSD) was found to be reduced by about a factor of 12 between 0% and 6% cross-linking. At longer times, the MSD exhibits a plateau-like behavior. The calculated incoherent dynamic structure factor  $S_s(Q,t)$ was observed not to be influenced by cross-links at high values of the momentum transfer Q, while at lower Qs, a significant reduction of the  $S_s(Q,t)$ -decay is observed.

The corresponding characteristic time increases linearly with cross-link density. The decrease in the stretching parameter  $\beta$  with cross-link density indicates increasingly heterogeneous dynamics. Some tiny contributions of the elastic incoherent structure factor (EISF) to the dynamic structure factor are visible even at high Q. At lower Qs, large EISF contributions are observed. Similar to experimental results by Tschoegl et al., <sup>12</sup> TTSP was found to be valid at the segmental scale but not at the scale of the chain.

Further simulations<sup>14</sup> of similar systems at cross-linker densities up to 7% support the results of Liu *et al.*<sup>14</sup> In addition, the relaxation behavior was further examined by mode-coupling theory and the Vogel–Fulcher–Tammann equation. Again, the results indicate that TTSP holds on the segmental length scale but fails on the scale of the chain.

Arbe *et al.* investigated single-chain polymeric nanoparticles (SCNPs), where cross-links are of purely intramolecular nature. Using quasielastic neutron scattering (QENS), they showed that the structure factor S(Q) and the structural relaxation at the maximum  $S(Q_{\text{max}})$  are unaffected by cross-links. However, collective phenomena become apparent at low Qs via a strong Q-dependence of the coherent time. Structural investigations by small-angle neutron scattering (SANS) led to a characteristic heterogeneity length of about 1 nm that might correspond to the length scale of an additional slow process detected by dielectric spectroscopy. Heterogeneities are provoked by the internal multiloop topology of the SCNPs.

To experimentally separate self and collective dynamics in a highly cross-linked 1,2 polybutadiene (1,2-PB) melt, we combined data from neutron scattering instruments with largely different sensitivities to incoherent scattering. Neutron spectroscopy has the unique advantage of allowing to investigate dynamics at the microscopic scale with both spatial and temporal resolution. The specific combination of conventional (TOF, BS) and spin echo spectrometers has the additional advantage to allow a separation between

coherent (collective) and incoherent (self) contributions. This is due to the intrinsic difference in how these two contributions are "seen" by the spectrometers: in the former case (TOF, BS), coherent and incoherent contributions sum up, while in NSE, the incoherent contribution comes with a factor of -1/3. The simultaneous fit of the data allows to disentangle the two contributions. Moreover, the combination of the three techniques allows to cover a wide range of time scales as necessary to separate, for example, slow matrix and fast cross-link dynamics.

As a reference, we also investigated the uncross-linked melt. Aiming for the cross-link dynamics, the 1,2-PB was deuterated (d1,2-PB), while the cross-links were hydrogenated. We note that the cross-links are spatially extended and might also be viewed as part of the network mesh. The following results stand out:

- (i) For the pure melt around the structure factor peak  $S(Q_{\max})$ , we observe clear De Gennes narrowing. Toward lower Qs, the collective relaxation time  $\tau_c(Q)$  continuously increases indicating an unusually large correlation length  $\xi_c$  for the cross-over to viscoelastic homogeneity. <sup>16</sup>
- (ii) In the highly cross linked d1,2-PB melt, the original structure factor peak of pure d1,2-PB is significantly reduced; instead,
- (iii) A strong new peak  $S(Q_{cross})$  emerges, which we assign to the correlation of the hydrogen containing cross-linkers;
- (iv) The collective d1,2-PB relaxation rate around the  $S(Q_{max})$  of the neat melt is retarded by nearly two orders of magnitude.
- (v) Compared to the pure melt, at  $S(Q_{cross})$ , the cross-link fluctuation rate is reduced by about three orders of magnitude.
- (vi) Finally, the cross-linking strands exhibit their own fast dynamics, which is well represented by diffusion within a sphere with a radius of  $R \cong 4$  Å.

#### II. THEORETICAL CONSIDERATIONS

#### A. Polymer dynamics: Rouse, cross-link motions

As a consequence of the high cross-link density, in our experiments the segmental dynamics on scales well below the entanglement distance are relevant.<sup>17</sup> There, if undisturbed, the 1,2-PB segments will follow Rouse dynamics. The MSD is sub-diffusive with

$$\langle \Delta r^2(t) \rangle = 2 l_{seg}^2 \left( \frac{3 k_B T t}{\pi \zeta l_{seg}^2} \right)^{\frac{1}{2}} = \left( \frac{4 W l_{seg}^4}{\pi} t \right)^{\frac{1}{2}}$$
, where  $l_{seg}$  is the segment length taken as the monomer size  $l$ ,  $k_B$  is the Boltzmann constant,  $T$  is the temperature and  $\zeta$  is the monomeric friction.  $W l^4 \equiv W l_{seg}^4$  is the so-called Rouse rate, which is measured directly by QENS. The incoherent scattering function relates to the MSD:  $l_{seg}^{18,19}$ 

$$S_{self}(Q,t) = \exp\left[-\frac{Q^2}{6} \langle \Delta r^2(t) \rangle\right]$$

$$= \exp\left[-Q^2 \left(\frac{Wl4t}{9\pi}\right)^{\frac{1}{2}}\right]$$

$$= \exp\left[-\left(\frac{t}{\tau_{self}(Q)}\right)^{\frac{1}{2}}\right], \qquad (1)$$

with  $\tau_{self} = \frac{9\pi}{Wl4Q^4}$ . Thus, the characteristic time for segmental diffusion follows a  $Q^{-4}$  law. The motion of cross-links has been treated

theoretically by Warner<sup>20</sup> and measured on the microscopic scale by Oeser *et al.*,<sup>21</sup> although for weakly cross-linked chains. As the theory predicted, the fluctuation rate of the cross-link was found to be retarded to  $2/(f\ W)$ , where f is the functionality of the cross-link.

The validity of the Rouse model at shorter scales is limited by the details of the chemical monomer structure and/or by the appearance of forces relating to interaction potentials not covered by random thermal forces. This regime shows itself by deviations from  $\tau(Q) \sim Q^{-4}$  toward smaller exponents and stretching exponents deviating from  $\beta = 1/2$ . In general, the Gaussian relationship  $\tau_{self}(Q) \sim Q^{-2/\beta}$  is violated, indicating that the system becomes heterogenous.

#### B. Collective dynamics in polymer melts

To model collective dynamics in the mesoscopic regime of liquid matter, Novikov *et al.* proposed a simple analytical formula that interrelates the viscoelastic homogenous regime with local diffusive motion:<sup>16</sup>

$$\frac{1}{\tau_c(Q)} = \frac{1}{\tau_\alpha(0)} \frac{K_B}{M_L} \exp\left[-Q^2 \xi_c^2\right] + \frac{1}{S(Q)} \frac{Q^2 D_s}{1 + Q^2 \xi_D^2}.$$
 (2)

The first part describes the non-diffusive Q-independent relaxation in the viscoelastic homogenous regime characterized by the relaxation time  $\tau(Q \to 0) = M_L/K_B\tau_\alpha(0)$  with  $K_B$  the bulk modulus and  $M_L \approx K_B + 4/3G$  the longitudinal modulus, where G is the elastic shear modulus and  $\tau_\alpha$  is associated with a  $Q \to 0$  structural relaxation time, reflecting the viscoelastic coupling of stress and density fluctuations. The low Q limit should hold at distances beyond which the liquid is viscoelastically homogeneous. The corresponding correlation length is denoted by  $\xi_c$ .

In the high wave vector regime approaching the nearest-neighbor distance (structure factor maximum), we expect diffusive properties exhibiting an incoherent structure factor as  $S_s(Q,t) \approx \exp\left[-Q^2D_s(Q)t\right]$ . For jump diffusion,  $D_s(Q)=1/\left(1+\left(Q\xi_D\right)^2\right)$  with  $\xi_D$  the jump length. Using the De Gennes narrowing approximation, the corresponding collective time amounts  $\tau_c^D(Q)=S(Q)\tau_s^D(Q)$  with  $\tau_s^D(Q)=(1+Q^2\xi_D^2)/(Q^2D_s)$ . Equation (2) interpolates between the two regimes.<sup>22</sup>

Colmenero et al. generalized Eq. (2) for polymer melts.<sup>23</sup> There, in general, we observe stretched exponential relaxation:

$$S(Q,t) \propto \exp\left[-\left(\frac{t}{\tau(Q)}\right)^{\beta}\right],$$
 (3)

where in the Gaussian regime,  $\tau_{self}(Q) \propto Q^{-\frac{2}{\beta}}$ ; finally,  $\tau_{self}(Q) = \tau_0 \left(1 + \frac{1}{Q^2 \xi_D^2}\right)^{\frac{1}{\beta}}$  leads to a generalization for anomalous collective motion as

$$\frac{1}{\tau_c(Q)} = \frac{1}{\tau_\alpha(0)} \frac{K_B}{M_L} \exp\left[-Q^2 \xi_c^2\right] + \frac{1}{S(Q)^{1/\beta}} \frac{D_s}{\xi_D^2} \left[1 + \frac{1}{Q^2 \xi_D^2}\right]^{-1/\beta}.$$
(4)

### C. Diffusive motion with spatial constraints: Volino model

Volino *et al.* considered a simple model for the diffusion of a particle in a Gaussian well confining the particle motion.<sup>24</sup> Unlike square well potentials, this model leads to simple analytical solutions for the incoherent dynamic structure factor. For a three-dimensional isotropic Gaussian well,

$$S_{self}(Q,t) = \exp[-(Qu)^2(1-\rho(t))],$$
 (5)

where u is the width of the Gaussian well and  $\rho(t)$  a relaxation function. Based on Volino's detailed comparison with the incoherent structure factor for diffusion within a hard sphere, the results for the Gaussian well and the diffusion within a sphere largely match if we choose  $R_{Vol}^2 \cong 5\langle u^2 \rangle$  and relate the diffusion constant  $D_s$  inside the sphere to the particle correlation time  $\tau_{Vol} = \langle u^2 \rangle/D_s = R_{Vol}^2/(5D_s)$  toward the Gaussian width  $\sqrt{\langle u^2 \rangle}$ . Then, Eq. (5) becomes

$$S_{self,Vol}(Q,t) = \exp\left[-(QR_{Vol})^2/5(1-\exp(-t/\tau_{Vol}))\right].$$
 (6)

Generalizing Eq. (6) for polymers, we introduce stretching  $\exp\left(-t/\tau_{Vol}\right) \to \exp\left(\left(\frac{t}{\tau_{Vol}}\right)^{\beta_{Vol}}\right)$ . For  $t\to\infty$ , Eq. (6) becomes the so-called elastic incoherent structure factor (*EISF(Q)* =  $\exp\left[-\frac{1}{5}(QR_{Vol})^2\right]$ ) mirroring the spatial extension of local diffusion.

#### **III. MATERIALS AND METHODS**

#### A. Polymer synthesis

#### 1. Materials

Dichloromethane (99.8%) was obtained from VWR. 2,2-Dimethoxy-2-phenylacetophenone (DMPA) (99%) and tri(ethylene glycol) dithiol (95%) were obtained from Sigma-Aldrich.

#### 2. Synthesis of d1,2-PB

The deuterated linear 1,2-PB sample (d1,2-PB) is identical to sample dPB5k-OH from Ref. 26, where the synthesis is described in detail.

#### 3. Synthesis of d1,2-PB cross-linked

The cross-linked 1,2-PB sample (d1,2-PBcross) was synthesized by cross-linking linear d1,2-PB with the hydrogenous cross-linker tri(ethylene glycol) dithiol using UV light and the photoinitiator DMPA (see Fig. 1). First, d1,2-PB was degassed under high vacuum conditions for 3 days. Inside a glove box, d1,2-PB (0.8250 g, 13.7 mmol carbon double bonds), tri(ethylene glycol) dithiol (0.2802 g, 1.54 mmol), and DMPA (0.1176 g, 0.459 mmol) were dissolved in 1.5 ml of dichloromethane inside a glass vial. The mixture was poured into an open flat neutron scattering container  $(30 \times 40 \text{ mm}^2)$ . The vial was washed with some extra dichloromethane to remove residual reaction mixture. The open neutron scattering container was left inside the glove box for 18 h to remove most of the solvent. This work was carried out in the dark to prevent cross-linking before solvent evaporation. The polymer was then cross-linked by illumination with UV light (Roschwege Star-UV385 UV-LED 385 nm) for 2 h. Outside the glove box, the sample was taken out of the neu-

**FIG. 1.** Cross-linking of d1,2-PB with the hydrogenous cross-linker tri(ethylene glycol) dithiol using UV light and the photoinitiator DMPA.

tron scattering container and shaken with 250 ml of toluene for one day to wash out DMPA residues. This process was repeated once with 50 ml of toluene for 3 h. After drying for 2 days under high vacuum, 1.042 g of sample d1,2-PBcross was obtained (calculated value: 0.8250 g d1,2-PB + 0.2802 g dithiol = 1.1052 g). The sulfur content in the sample was determined by elemental analysis to be 9.0 mass-%. The calculated value for the sample composition at 100% incorporation of the cross-linker was 8.9 mass-%.

#### **B.** Methods

#### 1. Neutron time-of-flight spectroscopy

Neutron time-of-flight experiments were performed at the IN5 spectrometer at the Institut Laue-Langevin (ILL).<sup>27</sup> The instrument was used at an incident wavelength of 6 Å, resulting in a nearly triangular resolution function with a width of about 0.045 meV. Samples (d1,2-PBc and d1,2-PBcross) were loaded in aluminum flat cells positioned at an angle of 135° with respect to the incident beam (the same cells and geometry were also used for measurements at the other spectrometers). Spectra were collected at four temperatures, namely, 5, 350, 375, and 413 K. A typical measuring time was 2 h. The low-temperature data were used to measure the resolution function in the chosen configuration. Data were corrected for empty cell scattering. Raw data reduction has been done using the open-source software LAMP.<sup>28</sup>

#### 2. Neutron backscattering spectroscopy

Neutron backscattering experiments were performed at the Emu spectrometer at the Australian Nuclear Science and Technology Organization (ANSTO) with a resolution of ~1  $\mu$ eV, equivalent to a time scale of ~1 ns (incident wavelength 6.3 Å).<sup>29</sup> The spectra were collected in the *Q*-range between 0.4 and 1.8 Å<sup>-1</sup> and exploiting the full energy transfer available ( $\pm$ 31  $\mu$ eV). Spectra were collected at one temperature for d1,2-PB (350 K) and three temperatures for d1,2-PBcross (5, 350, and 413 K). The typical measuring time was 12 h. A vanadium sample in the same flat geometry was measured to correct for detector efficiency. The measurement at 5 K

for d1,2-PB cross was used to determine the instrument resolution function. An empty flat container was measured in the same geometry and subtracted as background. Raw data were reduced using the open-source software Mantid.<sup>30</sup>

#### 3. Neutron spin echo spectroscopy

Neutron spin echo experiments were performed at the wideangle spin echo spectrometer WASP at ILL.<sup>31</sup> Unlike conventional spectrometers, neutron spin echo directly accesses the intermediate scattering function in the time domain, with relative weights of 1 for coherent and -1/3 for incoherent contributions to S(Q,t). The instrument was used with two different incident wavelengths: 7 Å, providing an accessible time range between 0.007 and 12 ns and a Q-range between 0.098 and 1.35 Å<sup>-1</sup> and 5 Å providing a time range between 0.003 and 5 ns and a Q-range between 0.14 and 1.89 Å<sup>-1</sup>. Samples were measured at three temperatures (350, 375, and 413 K).

#### 4. Data analysis

The simultaneous fit of IN5, Emu, and WASP data was performed using the software DATREAT, developed at the Jülich Centre for Neutron Science,<sup>32</sup> using methods described in Ref. 25 augmented with an additional branch for NSE data.

#### **IV. RESULTS**

#### A. Analysis of d1,2-PB

#### 1. Analysis of the static structure factor

We first analyze the WASP data of d1,2-PB at three temperatures ( $T=350,\ 375,\$ and 413 K). In Fig. 2(a), we report the coherent contribution as measured by WASP through polarization analysis, separating experimentally the incoherent contributions. Apart from the Debye–Waller factor, from the coherent contribution we directly obtain the static structure factor S(Q) (since the data are not on absolute scale, there is always an arbitrary factor upfront). Given that this sample was measured only at  $T=350\$ K on Emu, we estimated the Debye–Waller factor from that of the

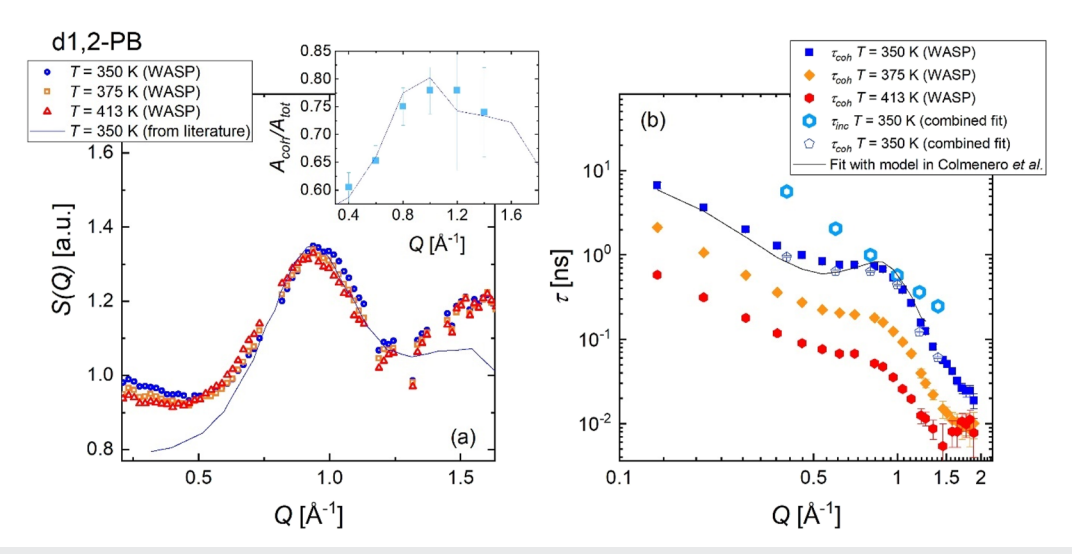


**FIG. 2.** (a) Static measurements on WASP. For T=350 K, the data of the static structure factor S(Q) from literature are also reported. In the inset, the ratio between coherent and total scattering  $A_{coh}/A_{tot}$  is reported, as obtained from the combined fit (symbols) and as calculated from the S(Q) from literature (line). (b) Relaxation times as obtained from the simultaneous fit of the data with both coherent and incoherent contributions (at T=350 K, open symbols) and by fitting the WASP data with only a coherent contribution (at all temperatures). The solid line is from the fit of  $\tau_{coh}$  at T=350 K according to the model in Eq. (4).

cross-linked sample measured on IN5. As may be seen seemingly, such obtained results are subject to a significant background that is particularly strong in the forward direction (see later). The Debye–Waller corrected values are in reasonably good agreement with S(Q) at  $T=350~\rm K$  from literature (rescaled by a suitable factor).<sup>33</sup>

#### 2. Fit of the WASP and Emu data

The knowledge of the chemical composition of the sample and the static structure factor S(Q) allows calculation of the coherent and incoherent contributions at each Q as  $\sigma_{coh}(Q) = S(Q) \cdot 0.52 \text{ cm}^{-1}$ and  $\sigma i_{nc}(Q) = 0.12 \text{ cm}^{-1}$  ( $\sigma = \sum n_i \sigma_i / V_{mol}$  with  $V_{mol} = M/\rho N_A$  and  $\rho = 0.96 \text{ g/cm}^{-3.34}$ ). This estimate shows that the coherent contribution to the spectra will dominate in the Q region around S(Q) at 1 Å<sup>-1</sup> [ $\sigma_{coh}(Q = 1 \text{ Å}^{-1}) = 0.48 \text{ cm}^{-1}$ ]. Moreover, on spin echo, the incoherent scattering component contributes to S(Q,t) with a factor of -1/3. To obtain preliminary information, we therefore fit the WASP data with a single stretched exponential to describe the coherent contribution only. At low Qs well below the structure factor maximum, the self (incoherent) contribution for polymer motion in the Rouse model assumes the form of a stretched exponential with  $\beta$  = 0.5. As discussed in the theory section, the pair correlation (coherent) contribution from a deuterated melt is not described by the Rouse model and has a more complex functional form. However, before testing more complex models, we assume that the coherent contribution can also be described by another stretched exponential. The spectra were best described using  $\beta_{coh} \approx 0.4$ . In fact, when left unconstrained, we found both  $\beta_{coh}$  and  $\tau_{coh}$  to be Q-dependent; however, the two parameters are strongly correlated. Moreover, at high Q, the values of  $\beta_{coh}$  have large uncertainties, as we only see the small tail of the relaxation function. To make the fit more robust,

we thus decided to fix  $\beta_{coh}$  to the average value of 0.4. The resulting relaxation times are reported in Fig. 2(b). The coherent time shows Arrhenius behavior, with an activation energy slightly higher than what is usually reported.<sup>35</sup> Other than for polyisobutylene,<sup>36</sup> no significant difference is found when calculating the activation energy in the peak region  $[E_{coh}~(0.9~\text{Å}^{-1})=500~\pm~50~\text{meV}]$  and well below it  $[E_{coh}~(0.14~\text{Å}^{-1})=520~\pm~60~\text{meV}]$ .

Information on the self-motion revealed by incoherent scattering may be obtained from the backscattering data (Emu). On the other hand, as we observe, the time scales for coherent and incoherent scattering in our sample are very close, and the fit of the Emu data alone also cannot separate the two contributions. The subsequent approach was fitting the WASP and Emu data simultaneously—the total scattering is given by  $I_{coh}$  +  $\sigma$   $I_{inc}$ —by using the same fitting parameters on both data sets and only varying the pre-factor of the incoherent contribution ( $\sigma = -1/3$  on WASP, +1 on Emu). These grossly different prefactors offer a unique opportunity to separate coherent and incoherent scattering experimentally. As described in the theoretical section, the dynamics of d1,2-PB segments can in principle be described by the Rouse model. However, deviations can be observed especially at high Qs, as one approaches scales small enough to see local effects. We thus use a generalized expression to describe both coherent and incoherent dynamics by using a sum of stretched exponential functions of the form  $e^{-\left(\frac{t}{\tau}\right)^{\beta}}$ . As mentioned above, for the incoherent term, this should give exactly the Rouse contribution when  $\beta$  = 0.5. The total fitting function included two stretched exponential terms, to describe coherent and incoherent dynamics, as well as a short-time incoherent term to describe fast processes observed on Emu as background, corresponding to a broad Lorentzian with a characteristic time  $\tau_{fast} \approx 1\text{--}10$  ps, which was fixed in the final fitting routine. In the time domain (WASP), the model function is

$$\frac{I(Q,t)}{I(Q,0)} = A(Q) \cdot \frac{A_1 e^{\left(-\left(\frac{t}{\tau_{coh}(Q)}\right)^{\beta_{coh}}\right)} - \frac{A_2}{3} e^{\left(-\left(\frac{t}{\tau_{inc}(Q)}\right)^{\beta_{inc}}\right)} - \frac{A_3}{3} e^{\left(-\left(\frac{t}{\tau_{fast}}\right)\right)}}{A_1 - \frac{A_2}{3} - \frac{A_3}{3}},$$
(7)

and in the frequency domain (Emu),

$$S(Q,\omega) = A(Q) \cdot FT \left[ \frac{A_1 e^{\left(-\left(\frac{t}{\tau_{coh}(Q)}\right)^{\beta_{coh}}\right)} + A_2 e^{\left(-\left(\frac{t}{\tau_{inc}(Q)}\right)^{\beta_{inc}}\right)} + A_3 e^{\left(-\left(\frac{t}{\tau_{fast}}\right)\right)}}{A_1 + A_2 + A_3} \right] \otimes R(Q,\omega), \tag{8}$$

where  $R(Q,\omega)$  is the resolution function and A(Q) is a fitted scaling

To reduce the number of free parameters, the self-dynamics was described by a power law<sup>37</sup>  $\tau(Q) = \tau_0 Q^{-b/\beta_{inc}}$ . The fixed, Q-independent parameters from the fit were  $\tau_0 = 0.58 \pm 0.09$  ns,

**TABLE I.** Parameters from the fit of d1,2-PB at T = 350 K using Eqs. (7) and (8). The coherent times at T = 375 and 413 K were obtained from the fit of the WASP data

	T =	350 K	T = 375 K	T = 413 K
$Q(\mathring{A}^{-1})$	$A_{coh}/A_{tot}$	$\langle  au_{coh} \rangle$ (ns)	$\langle  au_{coh} \rangle ( ext{ns})$	$\langle  au_{coh} \rangle ( ext{ns})$
0.4	$0.60 \pm 0.03$	$3.15 \pm 0.07$	$1.19 \pm 0.06$	$0.39 \pm 0.01$
0.6	$0.65 \pm 0.03$	$2.12 \pm 0.05$	$0.68 \pm 0.04$	$0.224\pm0.007$
0.8	$0.75 \pm 0.03$	$2.10 \pm 0.04$	$0.60 \pm 0.04$	$0.171 \pm 0.008$
1.0	$0.78 \pm 0.04$	$1.46 \pm 0.03$	$0.31 \pm 0.02$	$0.085 \pm 0.005$
1.2	$0.8 \pm 0.1$	$0.405 \pm 0.008$	$0.13 \pm 0.02$	$0.042 \pm 0.008$
1.4	$0.74 \pm 0.08$	$0.201\pm0.005$	$0.05 \pm 0.01$	$0.018\pm0.004$

 $b = 1.2 \pm 0.1$ ,  $\beta_{inc} = 0.5$ ,  $\beta_{coh} = 0.4$ ,  $\tau_{fast} = 5$  ps. The free, Q-dependent parameters, that is, the relative coherent scattering amplitude  $A_{coh}/A_{tot} = A_1/A_{tot} = 1 - A_{inc}/A_{tot}$  and the average coherent time  $(\langle \tau_{coh} \rangle \equiv \tau_{coh}/\beta_{coh}\Gamma(1/\beta_{coh})$ , where  $\Gamma$  is the Gamma function), are reported in Table I (the coherent times obtained from the fit of the WASP data only, at T = 375 and 413 K, are also reported). The resulting fitting functions, together with the experimental data, are shown for selected Qs for the WASP and Emu data, respectively, in Figs. 3(a) and 3(b). We observe very good agreement with the data points. Coherent and incoherent times obtained from the simultaneous fit of WASP and Emu are shown in Fig. 2(b), and the associated parameters in Table I. The coherent times at T = 350 K agree well with those evaluated by the fit of the WASP data only, further validating the goodness of the fit. Moreover, the ratio between coherent and total scattering agrees well with the one estimated theoretically. We note that the relative amount of coherent and incoherent scattering could be fixed by the "static" measurement on WASP, which in principle allows for polarization analysis. However, the uncontrolled background and loss of polarization prevent a quantitative determination of the amplitudes. Thus, we left the parameters unconstrained during the fit.

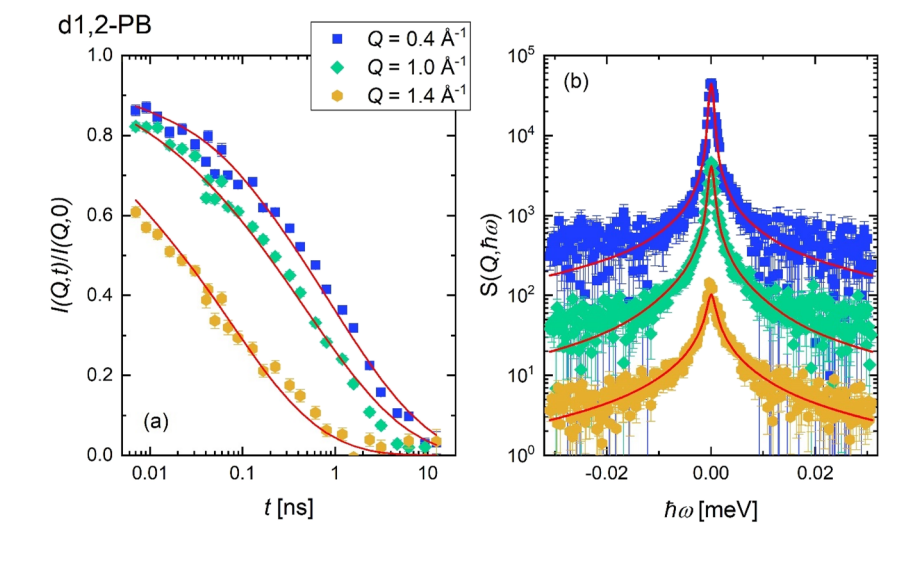
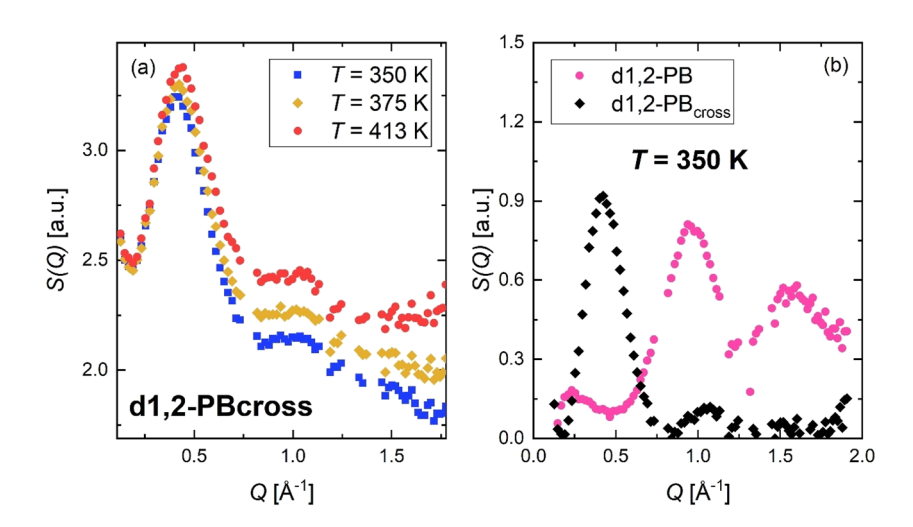


FIG. 3. Data collected on (a) WASP and (b) Emu at selected Qs, together with the corresponding fitting functions (solid lines).



**FIG. 4.** (a) Static measurements of d1,2-PB<sub>cross</sub> on WASP at different temperatures. (b) After subtraction of an estimated background, the data from d1,2-PB and d1,2-PB<sub>cross</sub> at  $T=350~{\rm K}$  are compared.

We now briefly discuss the observed collective- and self-dynamics. At high Q, both  $\tau_{coh}$  and  $\tau_{inc}$  follow a power-law decay  $\tau(Q)=\tau_0Q^{-b/\beta}$  with  $b\approx 1.2$ . This agrees with previous works  $^{35,37}$  and indicates that in this Q-range, the dynamics is heterogeneous and purely Gaussian behavior (where b=2) is not observed. As expected, the Rouse prediction of  $\tau(Q)\approx Q^{-4}$  does not adequately describe the relaxations at high Qs (short scales).

While for the self-dynamics we find a power-law dependence for  $\tau_{inc}$ , the coherent times display some structure in Q. Around  $S(Q_{\max} = 0.9 \text{ Å}^{-1})$ ,  $\tau_{coh}(Q)$  displays an intermediate maximum well known as De Gennes narrowing, occurring around the maximum of the structure factor peak. However, unlike polyisobutylene, <sup>36</sup> where at Q values below  $S(Q_{\max})$ ,  $\tau_{coh}(Q)$  assumes a plateau in Q, here for d1,2-PB  $\tau_{coh}(Q)$  significantly increases in the low-Q direction. We

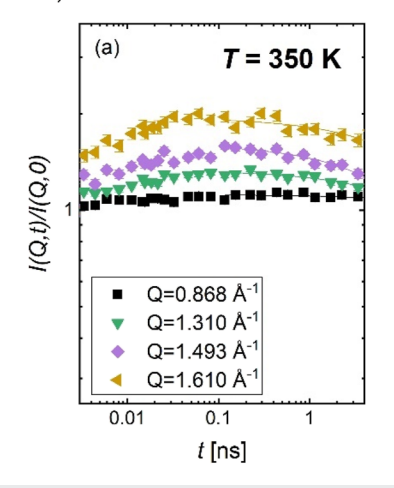
will examine in more detail the behavior of the coherent time in the discussion section.

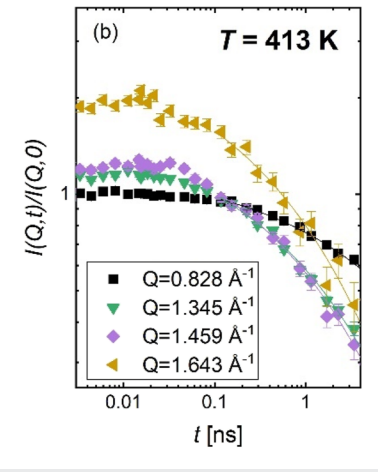
#### B. Results on d1,2-PBcross

#### 1. Analysis of the static structure factor

We now examine the case of d1,2-PB<sub>cross</sub>. In this sample, the hydrogenated cross-linker with a volume fraction of  $\phi_{cross} = 0.23$  significantly contributes to the signal. Due to the contrast with the deuterated d1,2-PB, at least at lower Q we expect to dominantly observe correlations between different cross-links. Similarly to the case of d1,2-PB, we start our analysis from an evaluation of the structure factor. Figure 4(a) displays the Debye–Waller factor corrected WASP data for three different temperatures. Other than for







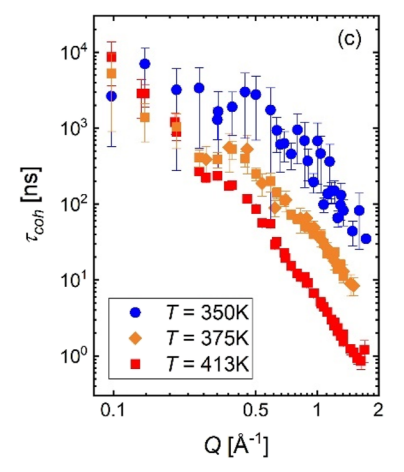


FIG. 5. [(a) and (b)] Scattering function on WASP, respectively, at T = 350 K and T = 413 K, at selected Qs. Solid lines are the corresponding fits with a stretched exponential. In (c), the resulting coherent relaxation times are reported.

TABLE II. Parameters from the fit of d1,2-PB<sub>cross</sub> using a single stretched exponential function

$Q(\mathring{A}^{-1})$	T = 350  K $\langle \tau_{coh} \rangle (\text{ns})$	T = 375  K $\langle \tau_{coh} \rangle (\text{ns})$	$T = 413 \text{ K}$ $\langle \tau_{coh} \rangle (\text{ns})$
0.4	$3000 \pm 1000$	800 ± 300	$570 \pm 70$
0.6	$1400 \pm 500$	$130 \pm 20$	$97 \pm 7$
0.8	$1400 \pm 600$	$100 \pm 20$	$36 \pm 3$
1.0	$700 \pm 300$	$52 \pm 7$	$16.1 \pm 0.9$
1.2	$230 \pm 50$	$27 \pm 4$	$8.4 \pm 0.7$
1.4	$70 \pm 20$	$13 \pm 3$	$4.1 \pm 0.6$

pure d1,2-PB, we observe a strong peak around  $Q = 0.45 \text{ Å}^{-1}$ , while the structure factor peak of neat PB is strongly reduced. The peak shows a nearly Gaussian shape, as also confirmed by preliminary SANS measurements on the same sample (data not reported). In Fig. 4(b), we compare S(Q) from d1,2-PB and d1,2-PB<sub>cross</sub> after subtraction of an estimated background. Apparently, due to the rather open incoming beam, a strongly enhanced background in the forward direction develops. While in this data presentation the low-Q peak in the d1,2-PB<sub>cross</sub> and the structure factor peak in d1,2-PB are of similar magnitude, it is evident that the main structure factor peak of 1,2-PB is strongly reduced in the cross-linked material, possibly indicating a loss of short-range order in the host matrix. Another possibility could be an impact of negative C–H and D–H correlations.

#### 2. Dynamics

For classifying the expectations for the dynamic studies, we may state the following: (a) from measurements of the relaxation dynamics around the region of  $Q \approx 1~\text{Å}^{-1}$ , we will get information on the effect of cross-linking on the dynamics of the host d1,2-PB matrix; (b) from measurements in the region around  $Q \approx 0.45~\text{Å}^{-1}$ , where the network specific correlation peak arises, we will observe the dynamics of cross-link–cross-link fluctuation. (c) In addition, studying the incoherent scattering, we access the hydrogen motion within the cross-linker.

a. Fit of the WASP data. For a first analysis of the cross-linked sample, we proceed as for d1,2-PB and first fit the WASP data only. We initially restrict our analysis to the (long-time) coherent contribution, and we thus fit each spectrum only for t > 0.1 ns with a single stretched exponential function. At T = 413 K, data were best fit with  $\beta_{coh}$  = 0.4. At lower temperatures, it is more difficult to obtain a conclusive determination of the fitting parameters, since the curves are almost flat and the relaxation times appear to be well beyond the time window of WASP [see Fig. 5(a) for the case of T = 350 K]. We found that data at T = 350 and 375 K are best described by  $\beta_{coh}$  = 0.6; however, uncertainties are much larger compared to the high temperature. The resulting relaxation times are reported in Fig. 5(c) and in Table II for selected Qs. The activation energy  $E_{coh}$  calculated at the maximum of the structure factor peak of d1,2-PB [ $E_{coh}$  ( $Q = 0.9 \text{ Å}^{-1}$ ) = 740 ± 70 meV] is larger than what is calculated for the non-cross-linked sample, indicating that the relaxation behavior is hindered, as also suggested by simulations.<sup>13</sup>

At all temperatures, around the maxima of S(Q) at  $Q \approx 0.45$  and  $Q \approx 1 \text{ Å}^{-1}$ , compared to neat d1,2-PB, an important slowing down

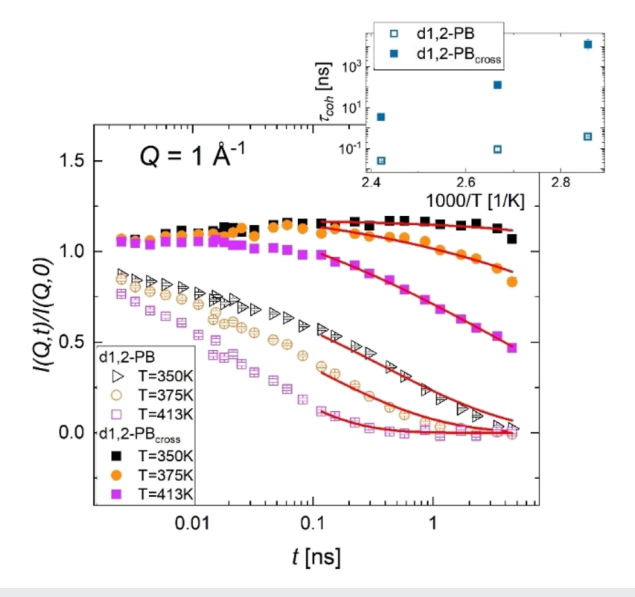


**FIG. 6.** Fit of the WASP scattering functions of d1,2-PB (open symbols) and d1,2-PB<sub>cross</sub> (full symbols) at Q=1 Å $^{-1}$ . The lines represent the fit results for t>0.1 ns (see text). In the inset, the corresponding relaxation times are reported.

is observed. While the latter is related to the PB matrix, the former will provide information on the correlation between cross-linkers. We will analyze the two *Q* regions separately.

b. Collective dynamics of the matrix ( $Q \approx 1.0 \text{ Å}^{-1}$ ). In Fig. 6, we compare the scattering functions of d1,2-PB and d1,2-PB<sub>cross</sub> at the

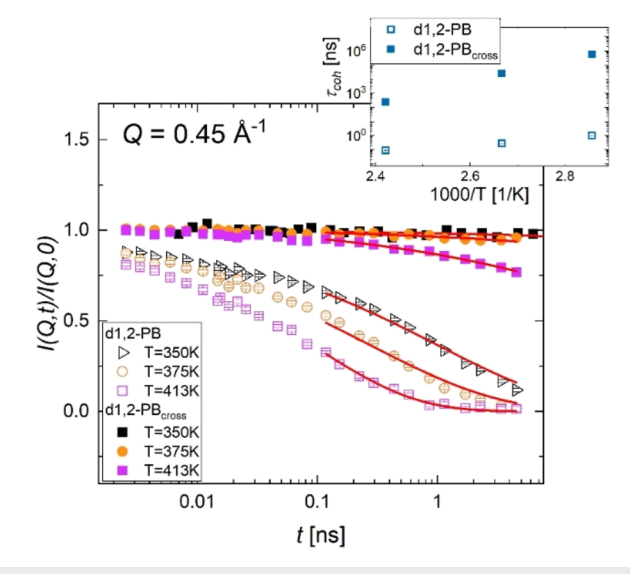


**FIG. 7.** Fit of the WASP scattering functions of d1,2-PB (open symbols) and d1,2-PB<sub>cross</sub> (full symbols) at  $Q = 0.45 \, \text{Å}^{-1}$ . The lines represent the fit results for t > 0.1 ns (see text). In the inset, the corresponding relaxation times are reported.

structure factor peak of d1,2-PB. We observe that the effect of cross-linking is to strongly slow down the dynamics of the matrix, roughly by two orders of magnitude (see inset).

c. Collective dynamics of cross-link fluctuations ( $Q \approx 0.45 \ \text{Å}^{-1}$ ). Figure 7 shows the comparison of the data on WASP of d1,2-PB and d1,2-PB<sub>cross</sub> at the low-Q structure peak. Here the dynamics of the cross-linked sample is even more strongly retarded, at all temperatures. The slowing down effect amounts to of about three orders of magnitude.

d. Simultaneous fit of IN5, Emu, and WASP (self-dynamics of the cross-link). Finally, we examine the incoherent scattering arising from the protons in the cross-linker, which provides information

about the hydrogen motion mainly within the cross-linker. To extract this contribution, we perform a simultaneous fit of IN5, Emu, and WASP data; that is, at each *Q*, a common set of stretched exponential functions is used to describe the data in all three experimental windows. Due to the confined dynamics, the incoherent contribution includes both an elastic and inelastic term. The elastic incoherent structure factor arises from the limited space within which the cross-links are able to move.

As a first step, we simultaneously fit the data from the three instruments (IN5, Emu, and WASP) at a fixed temperature using a model similar to that described in Eqs. (7) and (8). This time we also include an incoherent elastic term, such that the fitting function is written as

$$\frac{I(Q,t)}{I(Q,0)} = A(Q) \cdot \frac{A_1 e^{\left(-\left(\frac{t}{\tau_{coh}(Q)}\right)^{\beta_{coh}}\right)} - \frac{A_2}{3} e^{\left(-\left(\frac{t}{\tau_{inc}(Q)}\right)^{\beta_{inc}}\right)} - \frac{A_3}{3} - \frac{A_4}{3} e^{\left(-\left(\frac{t}{\tau_{fast}}\right)\right)}}{A_1 - \frac{A_2}{3} - \frac{A_3}{3} - \frac{A_4}{3}},$$
(9)

for the data in time space (WASP), and

$$S(Q,\omega) = A(Q) \cdot FT \left[ \frac{A_1 e^{\left(-\left(\frac{t}{\tau_{coh}(Q)}\right)^{\beta_{coh}}\right)} + A_2 e^{\left(-\left(\frac{t}{\tau_{inc}(Q)}\right)^{\beta_{inc}}\right)} + A_3 + A_4 e^{\left(-\left(\frac{t}{\tau_{fist}}\right)\right)}}{A_1 + A_2 + A_3 + A_4} \right] \otimes R(Q,\omega), \tag{10}$$

in the frequency domain (IN5, Emu). In the fitting routine, we fixed the coherent times to those obtained from the fit of the WASP data. We also fixed the values  $\beta_{inc}=0.5$ ,  $\beta_{coh}=0.6$  at T=350 K and 0.4 at T=413 K, and the fast background time  $\tau_{fast}=1$  ps. The free parameters in the fit are thus the amplitudes  $A_1=A_{coh}$ ,  $A_2=A^{inel}_{inc}$ ,  $A_3=A^{el}_{inc}$ ,  $A_4$ , and the incoherent relaxation times. The ratio between  $A_{coh}$  and  $A_{tot}\equiv A_{coh}+A^{el}_{inc}+A^{inel}_{inc}$  is plotted in Fig. 8(a). It qualitatively correlates with the maximum at  $Q\approx0.45$  Å $^{-1}$  observed in the static structure factor. The associated EISF  $\equiv A^{el}_{inc}/(A^{el}_{inc}+A^{inel}_{inc})$  is plotted in Fig. 8(b). The sharp drop to 0 of the EISF is quite unrealistic and probably determined by the fact that the fit cannot effectively discriminate between an elastic incoherent and a very slow inelastic coherent contribution. The incoherent times are plotted in the inset of Fig. 8(b). We observe that they are

much faster than the collective ones, indicating that they describe the fast self-motion of the cross-linker.

To achieve a better description of the incoherent contribution (self-correlation), we adopt the approach of Volino *et al.* that assumes a simple model for the confined motion of protons. <sup>24,25</sup> In this approach, we describe proton motion in terms of diffusion in a Gaussian well. The incoherent contribution in the time domain is expressed as  $f_{Vol}(Q,t) = \exp\{-Q^2R_{Vol}^2/5 \left[1-\exp(-(t/\tau_{Vol})^{\beta Vol})\right]\}$ , as described in the theoretical section. The total scattering function is thus written as

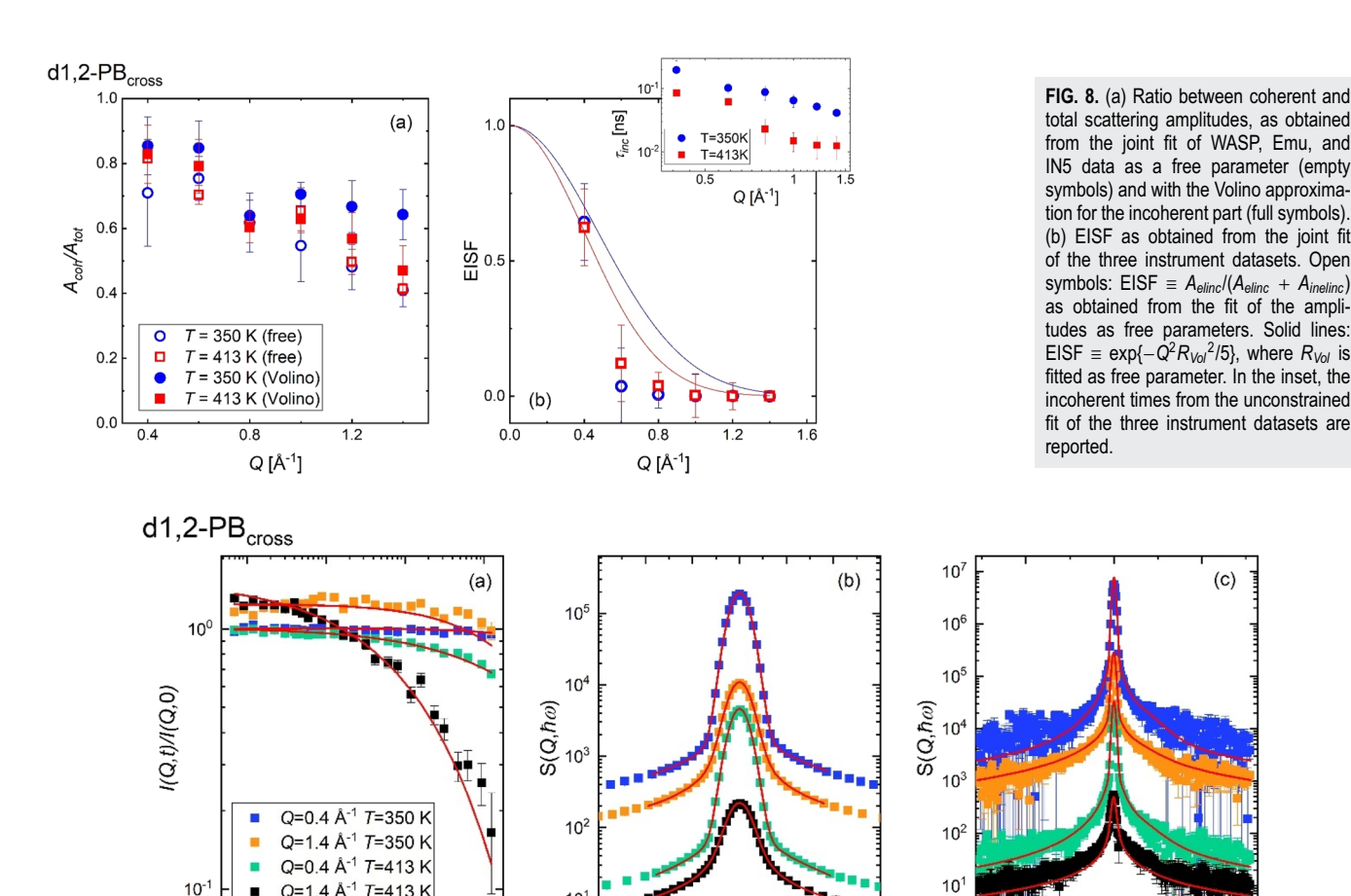
$$\frac{I(Q,t)}{I(Q,0)} = A(Q) \cdot \frac{A_1 e^{\left(-\left(\frac{t}{\tau_{coh}(Q)}\right)^{\beta_{coh}}\right)} - \frac{A_2}{3} f_{Vol}(Q,T) - \frac{A_3}{3} e^{\left(-\left(\frac{t}{\tau_{fast}}\right)\right)}}{A_1 - \frac{A_2}{3} - \frac{A_3}{3}},$$
(11)

in the time domain (WASP) and as

$$S(Q,\omega) = A(Q) \cdot FT \left[ \frac{A_1 e^{\left(-\left(\frac{t}{\tau_{coh}(Q)}\right)^{\beta_{coh}}\right)} + A_2 f_{Vol}(Q,T) + A_3 e^{\left(-\left(\frac{t}{\tau_{fast}}\right)\right)}}{A_1 + A_2 + A_3} \right] \otimes R(Q,\omega), \tag{12}$$

in the energy domain (Emu, IN5).

(c)



10

-0.3 -0.2 -0.1 0.0 0.1 0.2 0.3

10

FIG. 9. Comparison between the experimental data on (a) WASP, (b) IN5, and (c) Emu and corresponding to the common fitting functions in Eqs. (11) and (12) at selected Qs.

ħω [meV]

The resulting fitting functions are reported in Fig. 9 for selected Qs, and the corresponding parameters are listed in Table III (we fix  $\tau_{fast}$  = 1 ps). The data are well described across all three experimental windows. The ratio  $A_{coh}/A_{tot}$  qualitatively follows the measured S(Q). In addition, the description of the incoherent elastic part EISF =  $\exp\{-Q^2 R_{Vol}^2/5\}$  gives a more realistic trend as a function of Q [Fig. 8(b)]. The radius correlates with the radius of gyration  $R_g = 3.6$  Å, estimated for the cross-linker from the structural analysis. This is also consistent with the idea that the cross-linker

TABLE III. Parameters from the fit of d1,2-PBcross with the model described in Eqs. (11) and (12).

T(K)	$eta_{coh}$	$oldsymbol{eta}_V$	$ au_{Vol}$ (ns)	$R_{Vol}$ (Å)
350 413	0.6 0.4	0.5	$0.40 \pm 0.01 \\ 0.212 \pm 0.002$	$3.33 \pm 0.03$ $3.94 \pm 0.08$

motions extend to a characteristic distance close to the size of the

0.02

0.00

ħω [meV]

0.02

#### V. DISCUSSION

This work aimed at the experimental determination of self and collective dynamics in a highly cross-linked 1,2-PB rubber. Incoherent scattering, which directly measures the mean squared displacement of hydrogen atoms, contributes very differently to conventional quasielastic neutron scattering (factor 1) and neutron spin echo (factor -1/3). Using the NSE spectrometer WASP together with the time-of-flight spectrometer IN5 and the backscattering spectrometer Emu, we exploited this property to experimentally distinguish between the different coherent and incoherent scattering dynamics.

In the following, we first discuss the results on a pure, fully deuterated 1,2-PB melt, which was taken as reference. Thereafter, we highlight the essential results from the highly cross-linked melt and

0.01

0.1

t [ns]

finally discuss the internal dynamics within the spatially extended cross-linking strand.

#### A. 1,2-PB

The 1,2-PB or polyvinyl ethylene (PVE) has been studied before both by relaxational techniques such as dielectric spectroscopy and mechanical relaxation and also by incoherent QENS on hydrogenated 1,2-hPB. Alegría et al. investigated the relaxation of 1,2-PB by dielectric and mechanical means, establishing a Vogel-Fulcher (VF) description of the relaxation time as  $\tau_{VF}$  =  $1.03 \times 10^{-12} \exp\left[\frac{1020}{T-234.5}\right]$  [sec], which is valid near the glass transition temperature.<sup>38</sup> Narros et al.<sup>37</sup> reported QENS results revealing a stretched relaxation function with a stretching parameter  $\beta \cong 0.5$ . Due to the awkwardly shaped monomer deviations from Gaussianity  $(\tau_s \sim Q^{-2/\beta})$ , they found deviations already above  $Q \cong 0.5 \text{ Å}^{-1}$ . The relaxation time at  $Q = 1.0 \text{ Å}^{-1}$  and 418 K was reported as  $\tau_s$ ≅ 40 ps. Our results displayed in Fig. 2(b) lead to an estimated relaxation time of  $\tau_s \cong 30$  ps at 413 K. For the temperature dependence of the relaxation times, we observe an activation energy of about 500 meV, somewhat larger than an extrapolation of the low-temperature VF would predict. Taking the relaxation time at  $Q = 1.0 \text{ Å}^{-1}$  for a comparison with the dielectric results, the VF relation predicts  $\tau_s \cong 300$  ps about an order of magnitude slower than the neutron results—seemingly the VF equation cannot be extrapolated to the high temperatures, where the neutron data were taken.

To rationalize the collective relaxation times, we applied the approach of Eq. (4) proposed by Colmenero *et al.*, <sup>23</sup> where the authors describe the *Q*-dependence of the collective times in a polyisobutylene (PIB) melt. There, the salient features were a pronounced De Gennes narrowing around the structure factor peak and a plateauing of the collective times toward lower *Q*, which was termed typical for "intermediate" time- and length-scales larger than atomic dimensions, but smaller than the hydrodynamic limit.

We fit the data at T=350 K by fixing  $\xi_D$  to the characteristic jump distance for polybutadiene reported in the literature  $(\xi_D=0.5\ \text{Å})^{39}$  and  $\tau_\alpha(0)=8.24$  ns from dielectric spectroscopy. The resulting fitting function is reported in Fig. 2(b). The parameters from the fit are  $D_s=2.5\pm0.6\ \text{Å}^2/\text{ns}$ ,  $\beta=0.75\pm0.08$ , and  $\xi_c=6\pm2\ \text{Å}$ . However, the low Q data for  $\tau_c(Q)$  do not suggest the occurrence of a plateau. Therefore, due to the limited Q region accessed, a conclusive determination of  $\xi_c$  is prevented. The absence of a clear signature of a plateau in  $\tau_c(Q)$  indicates that for d1,2-PB the cross-over to viscoelastic homogeneity is realized only at fairly large length scales. We speculate that this larger length scale relates to the stiff and bulky monomer structure. The value for  $K_B/M_L$  is well within the expectation for a polymer melt, for example, for PIB,  $K_B/M_L=1.6$  is found. We have the strong distance of the strong polymer melt, for example, for PIB,  $K_B/M_L=1.6$  is found.

#### **B. 1,2-PBcross STRUCTURE**

The salient features of the 1,2-PB<sub>cross</sub> structure are the appearance of a strong correlation peak around  $Q \approx 0.45$  Å  $^{-1}$  and the important reduction of the 1,2-PB structure factor peak at  $Q \approx 1$  Å  $^{-1}$ . To elucidate the origin of the low-Q peak, we look in detail at the chemical structure of the sample (see Fig. 1): the crosslinking strand is built from 15 bonds, 4 of them result from the PB side groups, where by cross-linking the double bonds are converted to single bonds. From the sulfur analysis, we find that on

average every nine d1,2-PB bonds the host connects to a cross-linker. From the cross-linking strand, the inner part is protonated and the outer part on each side contains two deuterated  $CD_2$  groups and one sulfur atom. Thus, in the d1,2-PB environment, only the inner part is visible. Strictly speaking, we are not dealing with cross-linker dynamics but rather with the dynamics of the rubbery mesh, which is built by two labeled (hydrogenated cross-linker) strands together with two 1,2-PB strands each. Under these circumstances, the sharp correlation peak is rather unexpected.

The peak position is found at  $Q \approx 0.45 \text{ A}^{-1}$ , corresponding to an average distance of about 15 Å. Let us have a look at the other relevant distances in the rubber. The labeled part of the mesh strand resulting from the cross-linker involves seven bonds; assuming a coil conformation and taking  $C_{\infty} \cong 5$  (oxygen atoms in the chain), its radius of gyration  $R_g^2 = \frac{l_0^2 * C_{\infty} * N}{6} \cong \text{ or } R_g = 3.7 \text{ Å}$ ; the end to end distance  $R_e$  of the full cross-linker amounts to  $R_e^2 \cong l_0^2 * C_\infty * N$ . Taking  $C_{\infty} \cong 6$  (hydrocarbon bonds) and N = 15, we find  $R_e \cong 15$  Å. In this physical picture, the origin of the peak would lie in the fluctuations of the labeled cross-linker part of the mesh, which could be envisioned as little coils separated by a deuterated PB environment. The origin of the strong low-Q peak must be connected to the correlation between labeled network meshes. We also note that its position at  $Q \approx 0.45 \text{ Å}^{-1}$  correlates reasonably well with the volume fraction of cross-links contained in the sample. Its intensity arises from the important contrast between the hydrogenated cross-links, containing 14 protons and the deuterated d1,2-PB.

Inspecting Fig. 4(b), we realize a strong reduction of S(Q) in the region where pure d1,2-PB assumes its main structure factor peak. Obviously cross-linking at high cross-linker concentration significantly disturbs the local order of the d1,2-PB host.

#### C. 1,2 PB<sub>cross</sub> dynamics

The microscopic relaxation dynamics in highly cross-linked elastomers has mainly been accessed by MD simulations. With increasing cross-link concentration  $\phi_{cross}$ , Liu *et al.* found an increasingly reduced monomer diffusivity, which at 6% reaches one order of magnitude reduction compared to the corresponding uncrosslinked melt.<sup>13</sup> This retardation of diffusivity is accompanied by a broadening of the Kohlrausch-William-Watts (KWW) relaxation function. The calculated incoherent structure factor  $S_{self}(Q,t)$  is little affected at the monomer scale around the structure factor maximum and strongly retarded at low Q. At high  $\phi_{cross}$ , non-Arrhenius behavior becomes more pronounced. These observations are in line with our results on coherent scattering describing the collective dynamics. At the position of the structure factor maximum for the host, the collective relaxation times are observed to increase by two orders of magnitude. The observed temperature-dependent relaxation time in d1,2-PB<sub>cross</sub> is stronger than in the neat melt, indicating a stronger than Arrhenius behavior. Shen et al., again by MD simulations, observed a stretching parameter that with increasing  $\phi_{cross}$ was continuously diminishing.<sup>14</sup> Our results for the collective relaxation function do not support this finding: even at a much higher cross-link density, as Fig. 6 shows, the spectra from d1,2-PB and d1,2-PB<sub>cross</sub> are described by the same stretching parameter  $\beta \cong 0.4$ . We would like to stress here that self- and pair-correlation functions must not necessarily behave in the same way. We may also compare with previous NSE results on SCNPs<sup>15</sup> where the authors

find unaltered dynamics at the structure factor peak between cross-linked and uncross-linked chains. In our system, the much stronger cross-linking, on the contrary, induces a strong slowing down. It is interesting to note that Arbe *et al.* in the SCNPs also find a collective relaxation time increasing without plateauing toward low *Q*. They relate this observation to dynamic heterogeneity persisting to large spatial scales.

The well-developed cross-link-cross-link correlation peak allows us to address the cross-link fluctuations or the collective relaxation dynamics of the mesh. As seen from Fig. 7, the cross-link fluctuations are grossly retarded in time compared to the collective relaxation in the corresponding melt at the same Q-value. While for the two lower temperatures a relaxation is hardly detectable, at  $T=413~\rm K$  the measured relaxation time is about three orders of magnitude slower than in the neat melt. Thus, in highly cross-linked rubber, the prediction of Warner  $\tau_{cross}=\frac{2}{f}\tau_{Rouse}$  is not valid by far.

#### D. Internal cross-link dynamics

As the cross-linking agent by itself can be envisioned as a short polymer chain, we expect significant internal dynamics that, as a consequence of hydrogenation (the cross-link carries 14 protons), is well distinguishable in our experimental approach. As described in the results section, in a combined fit dwelling on the different sensitivity to incoherent scattering by NSE and direct spectrometers, we could well resolve the internal motion of the hydrogens of the cross-link strand. Using the Volino approach of Eq. (6) is fitting all spectra very well and leads to the structural and dynamical parameters of the Volino model of diffusion in a Gaussian well. The limiting radius for hydrogen diffusion of  $R_{Vol} = 4$  Å corresponds well to the radius of gyration of the visible cross-linker strand of  $R_g = 3.7$  Å. The corresponding time scale at 413 K of  $\tau_{Vol} = 0.2$  ns is significantly faster than that of the host  $[\tau_{coh}](Q =$  $(\mathring{A}^{-1}) = 16 \text{ ns}$ , indicating a dynamic decoupling of the observed motions.

#### VI. CONCLUSIONS

The combination of NSE, measuring S(Q,t), and conventional spectrometers, sensitive to  $S(Q,\omega)$ , leads to the unique opportunity to experimentally and quantitatively separate incoherent (self) motion and coherent (collective) motion with high-resolution neutron spectroscopy. We have studied a highly cross-linked 1, 2-PB network in comparison to a neat melt, demonstrating the novel experimental approach for high-resolution QENS. Recently, Arbe et al. 40,41 have applied a similar strategy investigating a simple liquid. To our knowledge, our work is the first on complex polymer dynamics, where this combined approach has been applied:

- (i) The results on the collective dynamics of neat 1,2-PB qualitatively support the analytical model for collective relaxation in a liquid by Novikov et al. and its extension to polymers by Colmenero et al., however, indicating an unusually large correlation length for the cross-over to viscoelastically homogeneous dynamics.
- (ii) At high cross-link density, a strong cross-link-cross-link correlation peak emerges; as in general, at high cross-link density,

- the network imperfections are reduced, we observe a nearly perfect Gaussian distribution of inter-cross-link spacings.
- (iii) Contrasting recent simulations, <sup>13,14</sup> we show that, at high cross-link density, the host dynamics on the segmental scale is strongly altered.
- (iv) The relaxations are greatly retarded but the stretching of the KWW function is not significantly altered compared to the neat melt.
- (v) Around the new inter cross-link correlation peak, we could directly access the very slow mesh fluctuations visualized by the inner part of the spatially extended cross-links.
- (vi) Finally, the cross-link strands exhibit their own dynamics that is much faster than that of the host (0.2 vs 16 ns) and could be well described by a model for diffusion in a Gaussian well.

With this demonstration of the capabilities achieved by a combination of S(Q,t) NSE and conventional  $S(Q,\omega)$  instruments, in the future we expect more of such studies on complex systems, even though the experimental effort is significantly more demanding than for standard experiments.

The experimental information obtained via our method can complement and validate computational results and shed light on the local arrangement and dynamics of the host polymer matrix and cross-linking points that directly impact the mobility of the rubber molecules at the microscopic scale. The mobility characteristics, in turn, reflect on the mechanical properties of the rubber, for example, under stress (temperature, pressure), whose knowledge has a tremendous impact on major industrial applications, including thermoelastomers or in the tire industry.

#### **ACKNOWLEDGMENTS**

The authors acknowledge the Australian Centre for Neutron Scattering and ANSTO for supporting the neutron research infrastructure used in this work via ACNS Proposal No. 15548, and the Institut Laue-Langevin for beamtime allocation. We kindly acknowledge Dr. Nicolas Martin at ILL for preliminary SANS measurements that were not included in the present work but contributed to the general understanding of the sample behavior. We also kindly acknowledge Dr. Reiner Zorn at JCNS for substantial help in reviewing data reduction and interpretation.

#### **AUTHOR DECLARATIONS**

#### **Conflict of Interests**

The authors have no conflicts to disclose.

#### **Author Contributions**

The manuscript was written through contributions of all authors. All authors have given approval to the final version of the manuscript.

**Benedetta P. Rosi**: Data curation (lead); Formal analysis (lead); Investigation (equal); Methodology (equal); Writing – original draft (equal); Writing – review & editing (equal). **Margarita Kruteva**:

Conceptualization (lead); Data curation (supporting); Investigation (equal); Methodology (equal); Supervision (equal); Writing – original draft (equal); Writing – review & editing (equal). Michael Monkenbusch: Data curation (supporting); Formal analysis (supporting); Methodology (supporting); Software (lead); Supervision (supporting); Validation (supporting); Writing – review & editing (supporting). Jürgen Allgaier Resources (equal); Writing – original draft (supporting). Peter Falus: Resources (equal); Writing – review & editing (equal). Jacques Ollivier: Resources (equal); Writing – review & editing (equal). Nicolas R. de Souza: Resources (equal); Writing – review & editing (equal). Dieter Richter: Conceptualization (supporting); Formal analysis (supporting); Methodology (equal); Supervision (equal); Validation (lead); Writing – original draft (lead); Writing – review & editing (equal).

#### **DATA AVAILABILITY**

Information on the availability of data collected at the ILL facility can be found at https://doi.org/10.5291/ILL-DATA.9-11-2082 and https://doi.org/10.5291/ILL-DATA.EASY-1281.<sup>27,31</sup>

#### REFERENCES

- <sup>1</sup>S. Kalakkunnath, D. S. Kalika, H. Lin, and B. D. Freeman, "Segmental relaxation characteristics of cross-linked poly(ethylene oxide) copolymer networks," Macromolecules **38**, 9679–9687 (2005).
- <sup>2</sup>K. Tsuchiya, K. Terada, Y. Tsuji, S. S. Y. Law, H. Masunaga, T. Katashima, T. Sakai, and K. Numata, "Cross-linking polybutadiene rubber via a thiol-ene reaction with polycysteine as a degradable cross-linker," Polym. J. **56**, 391–400 (2024).
- <sup>3</sup>S. Li, H. Zhao, T. Yue, L. Zhang, Y. Chen, and J. Liu, "All-atom molecular dynamics simulation of structure, dynamics and mechanics of elastomeric polymer materials in a wide range of pressure and temperature," Mol. Syst. Des. Eng. 9, 264–277 (2024).
- <sup>4</sup>R. Mashita, H. Kishimoto, R. Inoue, and T. Kanaya, "Small-angle x-ray and neutron scattering analyses of highly crosslinked rubber with unsaturated carboxylic acid," Polym. J. 45(1), 57–63 (2012).
- <sup>5</sup>O. Chaikumpollert, Y. Yamamoto, K. Suchiva, and S. Kawahara, "Mechanical properties and cross-linking structure of cross-linked natural rubber," Polym. J. 44(8), 772–777 (2012).
- <sup>6</sup>C. M. Roland, "Constraints on local segmental motion in poly(vinylethylene) networks," Macromolecules 27, 4242–4247 (1994).
- <sup>7</sup>N. M. Alves, J. L. Gómez Ribelles, J. A. Gómez Tejedor, and J. F. Mano, "Viscoelastic behavior of poly(methyl methacrylate) networks with different cross-linking degrees," Macromolecules 37, 3735–3744 (2004).
- <sup>8</sup>E. R. Duering, K. Kremer, and G. S. Grest, "Relaxation of randomly cross-linked polymer melts," Phys. Rev. Lett. **67**, 3531–3534 (1991).
- <sup>9</sup>D. R. Heine, G. S. Grest, C. D. Lorenz, M. Tsige, and M. J. Stevens, "Atomistic simulations of end-linked poly(dimethylsiloxane) networks: Structure and relaxation," Macromolecules 37, 3857–3864 (2004).
- <sup>10</sup>Z. Chen, C. Cohen, and F. A. Escobedo, "Monte Carlo simulation of the effect of entanglements on the swelling and deformation behavior of end-linked polymeric networks," <u>Macromolecules</u> 35, 3296–3305 (2002).
- <sup>11</sup>C. Svaneborg, R. Everaers, G. S. Grest, and J. G. Curro, "Connectivity and entanglement stress contributions in strained polymer networks," <u>Macromolecules</u> 41(13), 4920–4928 (2008).
- <sup>12</sup>N. W. Tschoegl, W. G. Knauss, and I. Emri, "The effect of temperature and pressure on the mechanical properties of thermo- and/or piezorheologically simple polymeric materials in thermodynamic equilibrium—A critical review," Mech. Time-Depend. Mater. **6**, 53–99 (2002).

- <sup>13</sup> J. Liu, D. Cao, and L. Zhang, "Static and dynamic properties of model elastomer with various cross-linking densities: A molecular dynamics study," J. Chem. Phys. 131, 34903 (2009).
- <sup>14</sup>J. Shen, X. Lin, J. Liu, and X. Li, "Effects of cross-link density and distribution on static and dynamic properties of chemically cross-linked polymers," Macromolecules **52**(1), 121–134 (2019).
- <sup>15</sup>A. Arbe, J. Rubio-Cervilla, A. Alegría, A. J. Moreno, J. A. Pomposo, B. Robles-Hernández, P. Malo De Molina, P. Fouquet, F. Juranyi, and J. Colmenero, "Mesoscale dynamics in melts of single-chain polymeric nanoparticles," <u>Macromolecules</u> 52, 6935–6942 (2019).
- <sup>16</sup>V. N. Novikov, K. S. Schweizer, and A. P. Sokolov, "Coherent neutron scattering and collective dynamics on mesoscale," J. Chem. Phys. 138, 164508 (2013).
- <sup>17</sup>L. J. Fetters, D. J. Lohse, D. Richter, T. A. Witten, and A. Zirkel, "Connection between polymer molecular weight, density, chain dimensions, and melt viscoelastic properties," Macromolecules 27, 4639–4647 (1994).
- <sup>18</sup>A. Wischnewski, M. Monkenbusch, L. Willner, D. Richter, and G. Kali, "Direct observation of the transition from free to constrained single-segment motion in entangled polymer melts," Phys. Rev. Lett. **90**, 058302 (2003).
- <sup>19</sup>M. Doi and S. F. Edwards, *The Theory of Polymer Dynamics* (Clarendon press Oxford, Oxford, 1986).
- <sup>20</sup>M. Warner, "The dynamics of particular points on a polymer chain," J. Phys. C: Solid State Phys. 14, 4985–4994 (1981).
- <sup>21</sup>R. Oeser, B. Ewen, D. Richter, and B. Farago, "Dynamic fluctuations of crosslinks in a rubber: A neutron-spin-echo study," Phys. Rev. Lett. 60, 1041–1044 (1988).
- $^{22}$ J. Colmenero, A. Alegría, A. Arbe, and B. Frick, "Correlation between non-Debye behavior and *Q* behavior of the α relaxation in glass-forming polymeric systems," Phys. Rev. Lett. **69**, 478–481 (1992).
- <sup>23</sup> J. Colmenero, F. Alvarez, Y. Khairy, and A. Arbe, "Modeling the collective relaxation time of glass-forming polymers at intermediate length scales: Application to polyisobutylene," J. Chem. Phys. 139, 44906 (2013).
- <sup>24</sup>F. Volino, J.-C. Perrin, and S. Lyonnard, "Gaussian model for localized translational motion: Application to incoherent neutron scattering," J. Phys. Chem. B 110, 11217–11223 (2006).
- <sup>25</sup> M. Monkenbusch, A. Stadler, R. Biehl, J. Ollivier, M. Zamponi, and D. Richter, "Fast internal dynamics in alcohol dehydrogenase," J. Chem. Phys. **143**, 075101 (2015).
- <sup>26</sup>M. Kruteva, M. Monkenbusch, A. Sharma, J. Allgaier, I. Hoffmann, B. Rosi, M. Dulle, L. Porcar, O. Matsarskaia, and D. Richter, "Unravelling chain confinement and dynamics of weakly entangled polymers in one component nanocomposites," Soft Matter (published online 2025).
- <sup>27</sup> M. Kruteva, J. Allgaier, B. Farago, M. M. Koza, M. Monkenbusch, J. Ollivier, D. Richter, and M. Zbiri (2023). "Local segmental dynamics in one component polymer nanocomposites," Institut Laue-Langevin (ILL), https://doi.org/10.5291/ILL-DATA.9-11-2082
- <sup>28</sup>D. Richard, M. Ferrand, and G. J. Kearley, "Analysis and visualisation of neutron-scattering data," J. Neutron Res. 4, 33–39 (1996).
- <sup>29</sup>N. R. de Souza, A. Klapproth, and G. N. Iles, "EMU: High-resolution backscattering spectrometer at ANSTO," Neutron News 27, 20–21 (2016).
- $^{30}\mathrm{Mantid},~Manipulation~and~Analysis~Toolkit~for~Instrument~Data,~Mantid~Project, 2013, http://dx.doi.org/10.5286/SOFTWARE/MANTID.$
- <sup>31</sup> M. Kruteva and P. Falus (2024). "Dynamics of cross-linked polybutadiene (PB)," Institut Laue-Langevin (ILL), https://doi.org/10.5291/ILL-DATA.EASY-1281
- <sup>32</sup>M. Monkenbusch, DATREAT, 2019, https://jugit.fz-juelich.de/neutrons/datreat.
- <sup>33</sup>T. Gkourmpis and G. R. Mitchell, "Experimentally driven atomistic model of 1,2 polybutadiene," J. Appl. Phys. 115, 53505 (2014).
- <sup>34</sup>L. J. Fetters, D. J. Lohse, and R. H. Colby, "Chapter 25 chain dimensions and entanglement spacings," in *Physical Properties of Polymers Handbook* (Springer, New York, 2007), pp. 445–452.

- <sup>35</sup>R. Zorn, A. Arbe, J. Colmenero, B. Frick, D. Richter, and U. Buchenau, "Neutron scattering study of the picosecond dynamics of polybutadiene and polyisoprene," Phys. Rev. E **52**, 781–795 (1995).
- <sup>36</sup>B. Farago, A. Arbe, J. Colmenero, R. Faust, U. Buchenau, and D. Richter, "Intermediate length scale dynamics of polyisobutylene," Phys. Rev. E **65**, 051803 (2002).
- <sup>37</sup>A. Narros, F. Alvarez, A. Arbe, J. Colmenero, D. Richter, and B. Farago, "Hydrogen motions in the α-relaxation regime of poly(vinyl ethylene): A molecular dynamics simulation and neutron scattering study," J. Chem. Phys. 121, 3282–3294 (2004).
- <sup>38</sup> A. Alegría, J. Colmenero, K. L. Ngai, and C. M. Roland, "Observation of the component dynamics in a miscible polymer blend by dielectric and mechanical spectroscopies," <u>Macromolecules</u> 27, 4486–4492 (1994).
- <sup>39</sup> J. Colmenero, A. Arbe, F. Alvarez, A. Narros, D. Richter, M. Monkenbusch, and B. Farago, "Hydrogen motions and the α-relaxation in glass-forming polymers: Molecular dynamics simulation and quasi-elastic neutron scattering results," Pramana 63, 25–32 (2004).
- <sup>40</sup> A. Arbe, G. J. Nilsen, M. Devonport, B. Farago, F. Alvarez, J. A. Martínez González, and J. Colmenero, "Collective dynamics and self-motions in the van der Waals liquid tetrahydrofuran from meso-to inter-molecular scales disentangled by neutron spectroscopy with polarization analysis," J. Chem. Phys. **158**, 184502 (2023).
- <sup>41</sup>A. Arbe, G. J. Nilsen, J. R. Stewart, F. Alvarez, V. G. Sakai, and J. Colmenero, "Coherent structural relaxation of water from meso—To intermolecular scales measured using neutron spectroscopy with polarization analysis," Phys. Rev. Res. 2, 022015(R) (2020).